Influence of addition of $CuO\text{-}BaCuO_2$ on microstructure of melt-textured $YBa_2Cu_3O_{7-\delta}$ ceramics and relevant transport properties*

J.M. Heintz, C. Magro, P. Dordor, D. Chateigner†, P. Germi†, M. Pernet†, D. Machajdik‡ and J.P. Bonnet**

Laboratoire de Chimie du Solide du CNRS, Université Bordeaux I, 351, Cours de la Libération, 33405 Talence Cedex, France
† Laboratoire de Cristallographie-CNRS, 38042 Grenoble Cedex 09, France
‡ Institute of Electrical Engineering, Slovak Academy of Sciences, Bratislava, Czechoslovakia
**ENSCI, 47 Avenue Albert Thomas, 87065 Limoges, France

The present work is devoted to the study of the relationship between microstructure and electrical transport properties in melt-textured $YBa_2Cu_3O_{7-\delta}$ ceramics. The production process described gives rise to a preferential orientation within large domains. SEM micrographs show long platelets stacked in a parallel arrangement. A.c. susceptibility measurements reveal a very low level of weak links. Direct and indirect critical current measurements, performed on long and small samples, respectively, reveal large differences. This discrepancy is ascribed to pseudo random orientation of the large domains, as confirmed by rocking curve characterizations. Pole figure measurements show that the preferential orientation of the free surfaces of the bulk sample appears to be ⟨113⟩ or ⟨103⟩ whichever face of the parallelepiped is considered. The latter observation is in agreement with the existence of non-coherent regions inside the sample. Consequently, a high critical current density (12 000 A cm^{-2}) can only be obtained for samples where long range texturing of the order of centimetres has been achieved.

Keywords: microstructure; $YBa_2Cu_3O_{7-\delta}$; transport properties

Sintering of $YBa_2Cu_3O_{7-\delta}$ under normal conditions (900–975°C) leads to the formation of granular and randomly orientated ceramics. Even though much progress has been made concerning the chemistry of the precursors needed to yield fine and high purity powders, the resulting ceramics still present relatively low values of critical current density ($J_c \approx 10^3$ A cm^{-2}) although the potential value for the $YBa_2Cu_3O_{7-\delta}$ phase is much higher. This behaviour is ascribed to the presence of weak link regions between the high J_c grains. Texturing of the microstructure can greatly reduce the weak link problem. Since 1988, many directional solidification techniques have been used to achieve textured ceramics[1–10], the latest using a magnetic field to enhance the texturing process[11,12]. The microstructural characterization of such ceramics is of interest for at least two reasons. First, the correlation between the production technique and the final microstructure could help us understand the mechanism of microstructure formation. Second, the study of the influence on the microstructure of chemical parameters such as the addition of CuO, $BaCuO_2$ or Y_2BaCuO_5 could allow us to control the development of texture and consequently to improve the transport properties[3,6,13,14].

This paper deals with the characterization of $YBa_2Cu_3O_{7-\delta}$ textured ceramics obtained using a controlled melt process without application of a thermal gradient. Since $YBa_2Cu_3O_{7-\delta}$ undergoes peritectic melting, both Y_2BaCuO_5 (211) precipitates and a liquid phase are formed above 1040°C under oxygen. Furthermore, the addition of $CuO\text{-}BaCuO_2$ offers a means by which to vary the quantity of the liquid phase and therefore the level of 211 phase in the system. The influence of this addition on the microstructure is investigated. A.c. susceptibility measurements are used to correlate transport properties to the change in microstructure.

Experimental procedure

Production process

The starting material is a Rhône–Poulenc powder. Three types of samples were prepared: type A corresponds to the stoichiometric composition; type B is a

* Paper presented at the conference 'Critical Currents in High T_c Superconductors', 22–24 April 1992, Vienna, Austria

0011–2275/93/030270–07

mixture of $YBa_2Cu_3O_{7-\delta}$ and 5 mol% CuO and $BaCuO_2$; and type C is a mixture of $YBa_2Cu_3O_{7-\delta}$ and 10 mol% CuO and $BaCuO_2$. The CuO used was a pure commercial powder (Prolabo, 99%) and the $BaCuO_2$ was obtained by a solid state reaction between $BaCO_3$ (Carlo Erba 99%) and CuO at 950°C.

The powders were pressed uniaxially at 70 MPa to form a parallelepiped bar ($5 \times 10 \times 80$ mm^3). This bar is put on to small yttria ceramic substrate samples inside a large alumina crucible. The Y_2O_3 substrates have been previously sintered for 6 h at 1460°C giving a porous material. The whole system is placed in the isothermal zone of a tubular furnace. No thermal gradient is superimposed. However, due to the configuration of the furnace and the length of the bar (8 cm), small differences in temperature could exist. The sintering schedule is given in *Figure 1*. The whole process is conducted under oxygen. Between 905 and 330°C, the cooling rate is slow (6°C h^{-1}) and a reoxidation annealing appears not to be necessary. The 6 h holding of the samples at 920°C is used to enhance the density before the melt process. Note that the samples are held for a comparatively short time (≈ 10 min) above the peritectic temperature.

Characterization techniques

The concentration of holes, referred to here as Cu^{3+}, expressed in moles per gram of total material was determined by a Mohr salt titration[15]. Microstructural observations were made using scanning electron microscopy (SEM), usually on polished samples, and scanning transmission electron microscopy (STEM) at 120 kV. The texturing of the melt process ceramics was checked either by pole figures or rocking curve measurements. A.c. susceptibility measurements were carried out to compare the transport properties of the different specimens and to give an estimation of critical current densities, using the Bean model.

Microstructural observations

The microstructure of a typical sample is presented in *Figure 2a*. Long parallel 'lines' clearly reveal the texturing, which is thought to be parallel to the (001) plane[16].

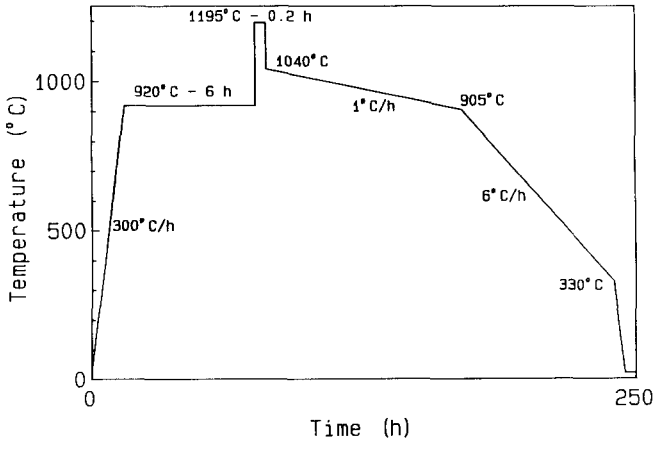

Figure 1 Schematic representation of the heating treatment under oxygen

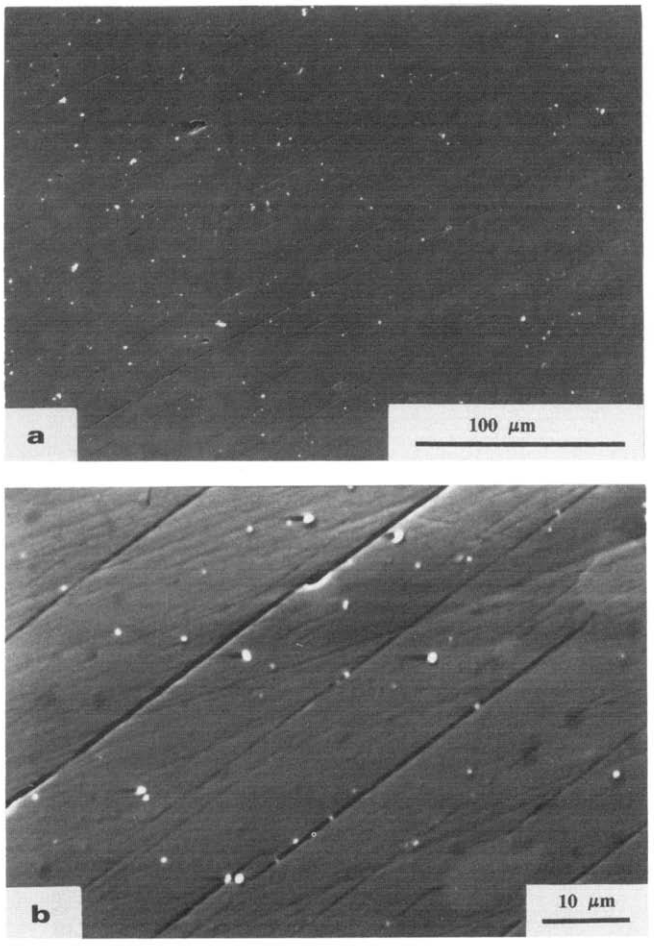

Figure 2 (a) SEM micrograph of typical texture of a melt process ceramic. (b) Higher magnification revealing the production fissures lying parallel to one another in the material

In fact, the parallel platelets cannot be considered to be grains in the usual sense. The lines between the platelets look more like cracks than grain boundaries (*Figure 2b*). Careful investigation of these defects at a higher magnification reveals traces of a residual liquid phase in some places (*Figure 3*). The cracks are likely to be the result of the texturing process (and will, therefore, be referred to as 'production fissures' in the following text). They reveal the places where the last remains of liquid were before complete solidification (to give $YBa_2Cu_3O_{7-\delta}$) and/or flowing in of the Y_2O_3 substrates. This interpretation is confirmed by a study of a quenched sample (from 980 to 20°C) which reveals large channels filled by a Cu- and Ba-rich phase (using EDX analysis) inside a $YBa_2Cu_3O_{7-\delta}$ crystalline domain (*Figure 4*).

Many impurities are present in these textured ceramics. Y_2BaCuO_5 is the main secondary phase. The 211 volumic concentration is estimated at 10% in sample A, where the grains, which are spherical or needle-like, are uniformly distributed. The grain size is usually >1 μm (*Figure 5*). The large quantity of 211 left behind during the production of $YBa_2Cu_3O_{7-\delta}$ is mainly due to the disappearance of part of the liquid phase at the bottom of the experimental system. According to the phase diagram, a liquid rich in CuO and $BaCuO_2$ exists above 920°C. This type of mixture is also known to be non-viscous. Consequently, it could flow easily and react

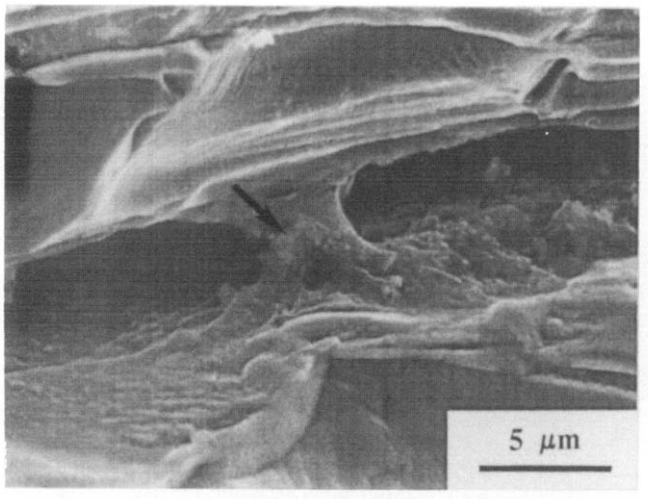

Figure 3 SEM micrograph of a fissure showing traces of a residual liquid phase (Cu- and Ba-rich)

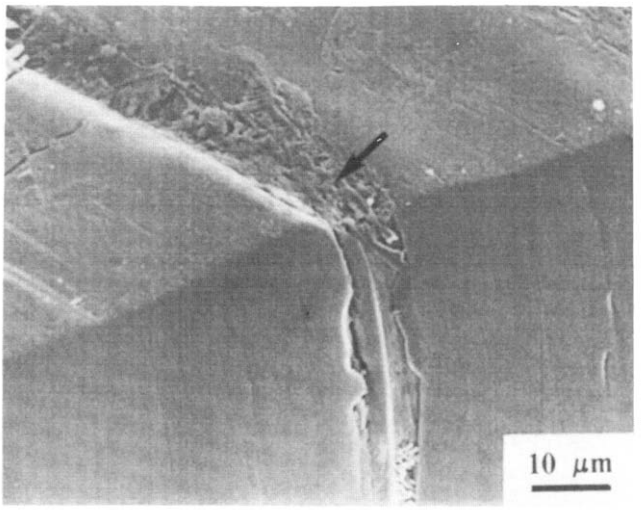

Figure 4 SEM micrograph of the edge of a quenched sample (980°C). The upper part of the micrograph is a free surface. The channel between the two $YBa_2Cu_3O_{7-\delta}$ blocks is filled by a Cu- and Ba-rich phase

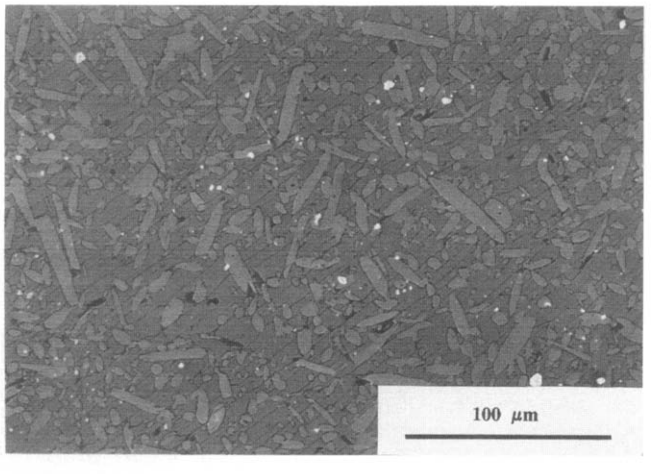

Figure 5 SEM micrograph showing the Y_2BaCuO_5 precipitates (spherical and needle-shaped grains) in a textured domain

with the Y_2O_3 substrates, giving rise to 211 and $YBa_2Cu_3O_{7-\delta}$ phases. As the peritectic reaction is incomplete, an excess of Y_2BaCuO_5 is left in the material. X-ray analysis of the Y_2O_3 substrates after ceramic processing shows the presence of the two phases mentioned.

Other impurities are found in the final ceramic including CuO (*Figure 6*) and $BaCuO_2$ grains, which are preferentially located near the ends of the samples. Type B or C ceramics contain more CuO inclusions and less 211 grains, in agreement with the composition of the starting mixture.

The thickness of the platelets (i.e. the average distance between fissures) seems to be related to the starting composition (*Table 1*). The more CuO-$BaCuO_2$ is added to the stoichiometric compound, the thicker the platelets. Moreover, CuO-$BaCuO_2$ addition strongly reduces the amount of residual 211 grains, which is in agreement with the phase diagram. Therefore interaction between fissures and the green phase has to be considered. SEM investigations have been used to support the final correlation. A micrograph of a quenched sample, presented in *Figure 7*, shows an area where $YBa_2Cu_3O_{7-\delta}$ is growing. The non-polished part in the background corresponds to a Ba- and Cu-rich phase (liquid phase). A 211 grain is located between two $YBa_2Cu_3O_{7-\delta}$ needles in the process of formation. Y_2BaCuO_5 is consumed to form $YBa_2Cu_3O_{7-\delta}$ until no liquid phase is left. The possible void left by the eventual disappearance of the liquid will be located on the path of or close to the 211 grain. Due to the difference in thermal expansion coefficients, a crack can appear and propagate during cooling in the growing fissure. The pattern of parallel fissures observed in the final material is almost certainly related both to the amount of the green phase during the melt stage and to the rate of consumption of the liquid phase during the solidification or its flowing down into the substrates. This interpretation is also supported by the study of McGinn *et al.*[13] on the microstructure of a zone melt-textured $YBa_2Cu_3O_{7-\delta}$ with 211 additions. They found that the $YBa_2Cu_3O_{7-\delta}$ platelet thickness decreased with an increase in 211 additions.

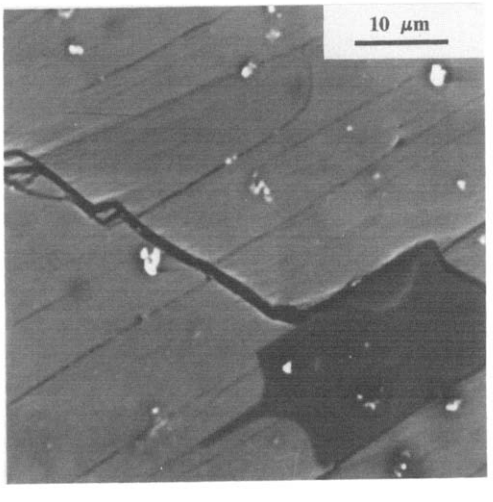

Figure 6 CuO inclusion (dark grain)

Table 1 Chemical, microstructural and magnetic characteristics of the melt-textured ceramics

Sample type	A	B	C
Initial composition	$YBa_2Cu_3O_{7-\delta}$	$YBa_2Cu_3O_{7-\delta}$ + 5 mol% CuO, $BaCuO_2$	$YBa_2Cu_3O_{7-\delta}$ + 10 mol% CuO, $BaCuO_2$
Average distance between cracks (μm)	5 – 20	5 – 40	>40
Random cracking	Not very important	Yes	Important
Cu^{3+} concentration (mol g^{-1})	7.61×10^{-4}	7.39×10^{-4}	6.16×10^{-4}
T_c onset (K)	92.9	93	92.9
$\Delta T_{50\%\chi'}$ (K)	1.18	0.52	0.67
$\Delta T_{80\%\chi'}$ (K)	1.86	0.88	1.24

The composite structure of these ceramics implies the presence of numerous stresses during the cooling process. Production fissures are a good way to relax such strains. On the other hand, in samples B and C, where the amount of green phase and the density of production fissures are low, the development of another type of crack is favoured. This is actually observed in *Figure 8*, where many random cracks compensate for the larger distance between parallel fissures. A third type of crack to mention is that due to the interaction between the flowing liquid phase and the porous Y_2O_3 substrates. These cracks grow perpendicularly to the substrates, as can be seen in *Figure 9*.

TEM observations show, in some places, the existence of either residual amorphous phases (sample A, *Figure 10*) or low angle grain boundaries (samples B or C) between production fissures. On a finer scale, lattice distortions have been revealed by non-homogeneous lightning in dark field conditions. This phenomenon has also been observed in non-textured $YBa_2Cu_3O_{7-\delta}$ ceramics[17].

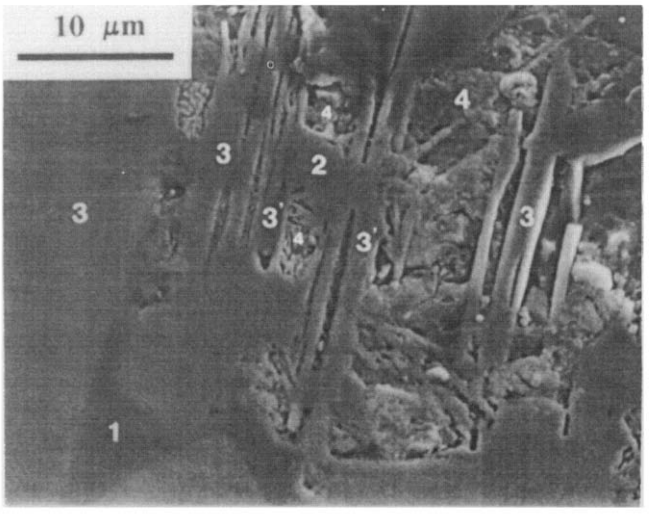

Figure 7 SEM micrograph of a polished section of a quenched sample (980°C) revealing the formation of $YBa_2Cu_3O_{7-\delta}$. Numbers correspond to areas of different chemical composition determined by EDX: 1, CuO; 2, Y_2BaCuO_5; 3, $YBa_2Cu_3O_{7-\delta}$; 4, Cu- and Ba-rich phase. Two $YBa_2Cu_3O_{7-\delta}$ needles (3') are growing from the reaction between Y_2BaCuO_5 (grain 2) and the liquid phase (4)

X-ray pole figures performed on the free surfaces of a large sample (schematically shown in *Figure 11*) confirm the strong orientation of the crystallites. The poles reform to points (i.e. with no dispersion) in the stereographic projection (*Figure 12*). The *c*-axis is not perpendicular to the surface, as can be seen in *Figure 12a* where the (007) pole is not centred. *Figure 12b* shows the stereographic projection of the (006) + (020) + (200) lines. It forms a well defined triangle with the central axis corresponding to ⟨113⟩. The same observations are made for surfaces a and b2 (*Figure 11*) when surface c presents a ⟨103⟩ preferential orientation. Added together, these results allow us to conclude that the surfaces are well textured. Nevertheless, as the same orientation is observed for two perpendicular faces (a and b), it is clear that the texture inside the bulk ceramic is not unique.

Rocking curves have been used to determine the texturing and its eventual modification from place to place within the heart of the material. Repeated X-ray diffraction measurements have been performed on the same sample (type B) but with a slight sweep of the tilt angle, ω, between the diffraction planes and sample surface. The obtained patterns are consistent with the existence of coherent domains a few microns long, in which the

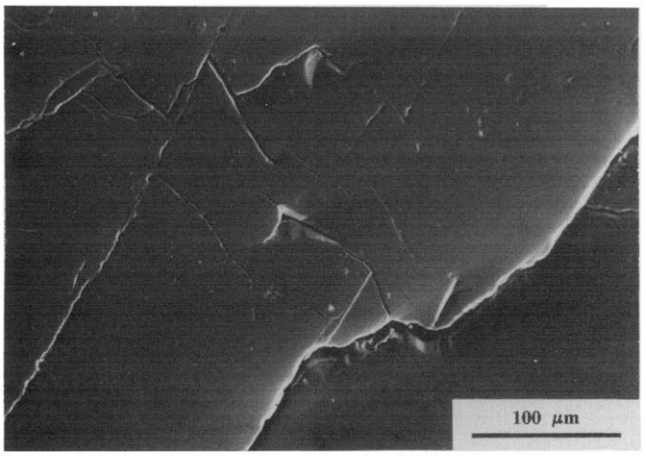

Figure 8 SEM micrograph of a type C ceramic showing the large distance between production fissures together with many random cracks

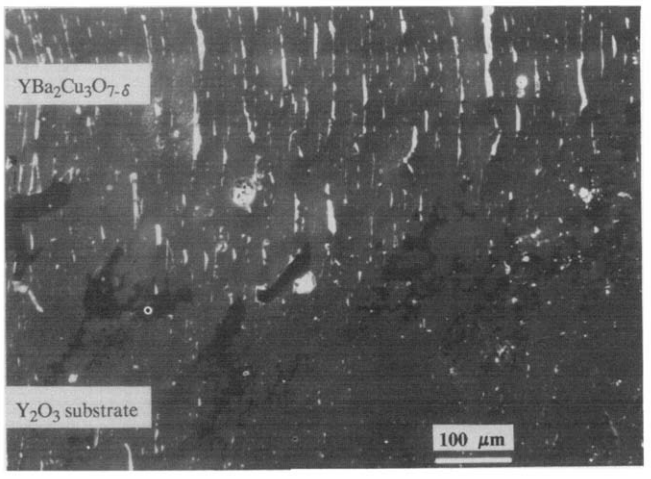

Figure 9 SEM micrograph of parallel cracks corresponding to the interaction of the ceramic with the porous Y_2O_3 substrates

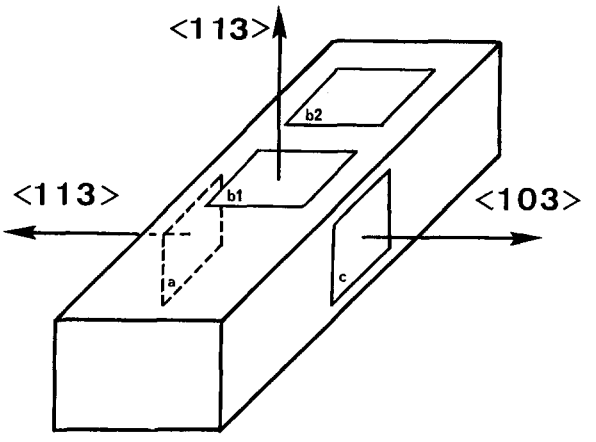

Figure 11 Schematic representation of the orientation of the free surfaces of a large ceramic sample. The zones investigated by X-ray diffraction pole figures correspond to the areas marked a, b1, b2 and c

preferential orientation remains within a $\pm 1.5°$ range. These coherent domains apparently give rise to larger blocks (≈ 100 μm long) where the orientation fluctuation is $<4°$. Strong and erratic pattern anomalies suggest that, over the whole sample, the blocks are subject to little orientation. This texture analysis is confirmed by SEM observations (*Figure 13*) and is coherent with the pole figure interpretation. The lack of a driving force, such as a thermal gradient or a magnetic field, during the melt stage and the recrystallization probably prevents a long range structure from forming.

Transport properties

A.c. susceptibility measurements ($\chi_{a.c.} = \chi' - i.\chi''$) have been carried out at 333 Hz using a mutual inductance bridge. Samples were cut in a parallelepiped shape ($1.8 \times 1.8 \times 7$ mm^3), so that their long axis lies parallel to the direction of the fissure. A.c. inductions with an amplitude of $0.01-1$ mT were applied parallel to the longest dimension of the samples. The presence of 211 phase actually reduces the superconductive volume and the $\chi_{a.c.}$ signal. Nevertheless, the 211 particles are more or less homogeneously distributed throughout the superconductive material, so the shielding currents can efficiently mask their presence.

Figures 14a, b and *c* show the response of samples A, B and C, respectively. The widths of the susceptibility dependence with the applied magnetic induction (from 0.01 to 1 mT), taken at 50 and 80% of the complete transition, are given in *Table 1*. Onset transition temperatures appear to be identical whatever the type of sample (*Table 1*), indicating that in each material the same maximum oxygen concentration is reached, at least in some separated domains. A sharp superconductive transition is observed for all ceramics. In contrast to the behaviour of fine grain ceramics processed by solid

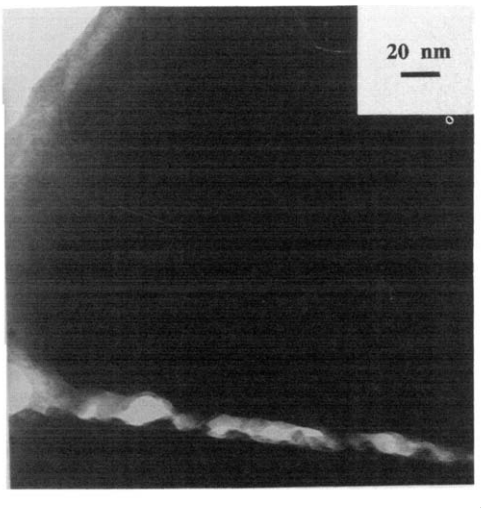

Figure 10 TEM micrograph of a type A sample revealing the existence of a residual amorphous phase between production fissures

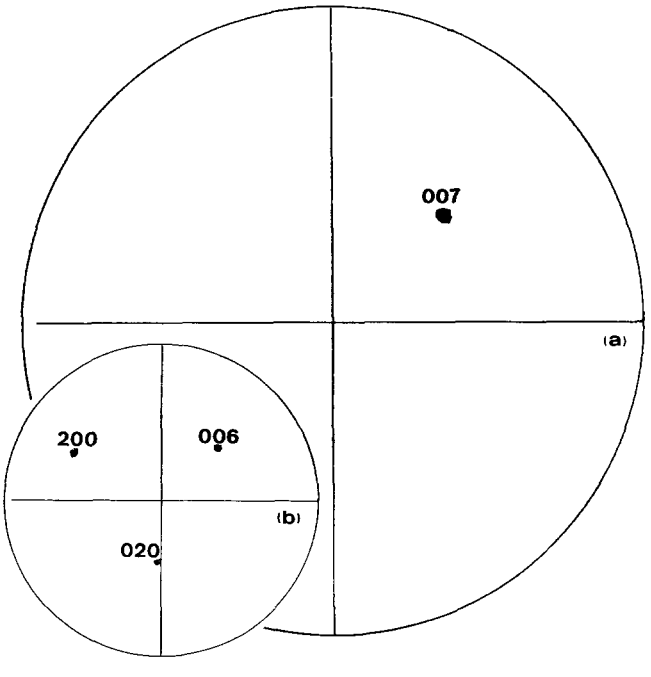

Figure 12 (a) 007 pole figure measured on the (b1) surface. (b) 200 + 020 + 006 pole figure measured on the (b1) surface

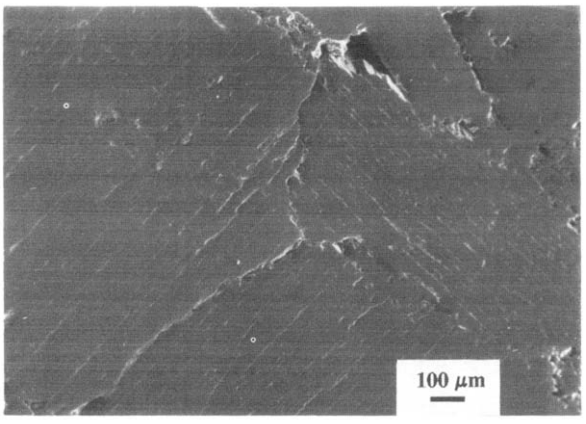

Figure 13 SEM micrograph of the inside of a type C ceramic showing at least three different large textured domains

state sintering, no intergranular effect is observed. This unique transition is attributed to intragranular behaviour, meaning that these materials could be considered to be large crystals. This corresponds to the previous analysis, suggesting that the lines delimiting the so-called platelets are not grain boundaries.

With decreasing temperature the susceptibility behaviour starts to change with sample type. In type A ceramics submitted to a low induction amplitude ($B_{ac} < 0.5$ mT), a shoulder can be seen in the imaginary part of the susceptibility. This shoulder could be attributed to weak link-like behaviour, related to the presence of the amorphous phases observed in TEM, or to defect zones around the production fissures. The lack of χ' anomaly indicates that the volume of defects remains very low. This contribution increases the sensitivity of the material to magnetic induction. As a consequence, maxima of χ'' appear at lower temperatures for type A samples than for type B or C samples. In other words, the critical current density, J_c, is, in this instance, partially limited by the defect area.

To describe how these defects are related to the fissures and how they help to increase the transition, measurements of susceptibility anisotropy have been performed. A small cubic sample ($1.8 \times 1.8 \times 1.8$ mm^3) was cut and the magnetic induction ($B \leq 1.5$ mT) applied parallel or perpendicular to the fissure direction. As for single crystals, the anisotropic factor remains low when small induction amplitudes are applied. Nevertheless, the transition width is larger when the shielding currents flow perpendicularly to the fissure network, showing the association between fissures and defects. Our results are in agreement with the results of McGinn[13]: an increase in the production fissure density corresponds to a decrease in J_c obtained either from magnetization or transport measurements. In the type A material where the distance between production fissures is $\approx 5-10$ μm, the oxygenation is assumed to be fairly homogeneous and the tail observed in the transition is mainly attributed to intradomain defects.

Type B ceramics exhibit the steepest and narrowest transition, suggesting the existence of an optimum amount of additives. No weak link type behaviour effect is observed in the imaginary part for type B or C materials. However, type C is characterized by a larger

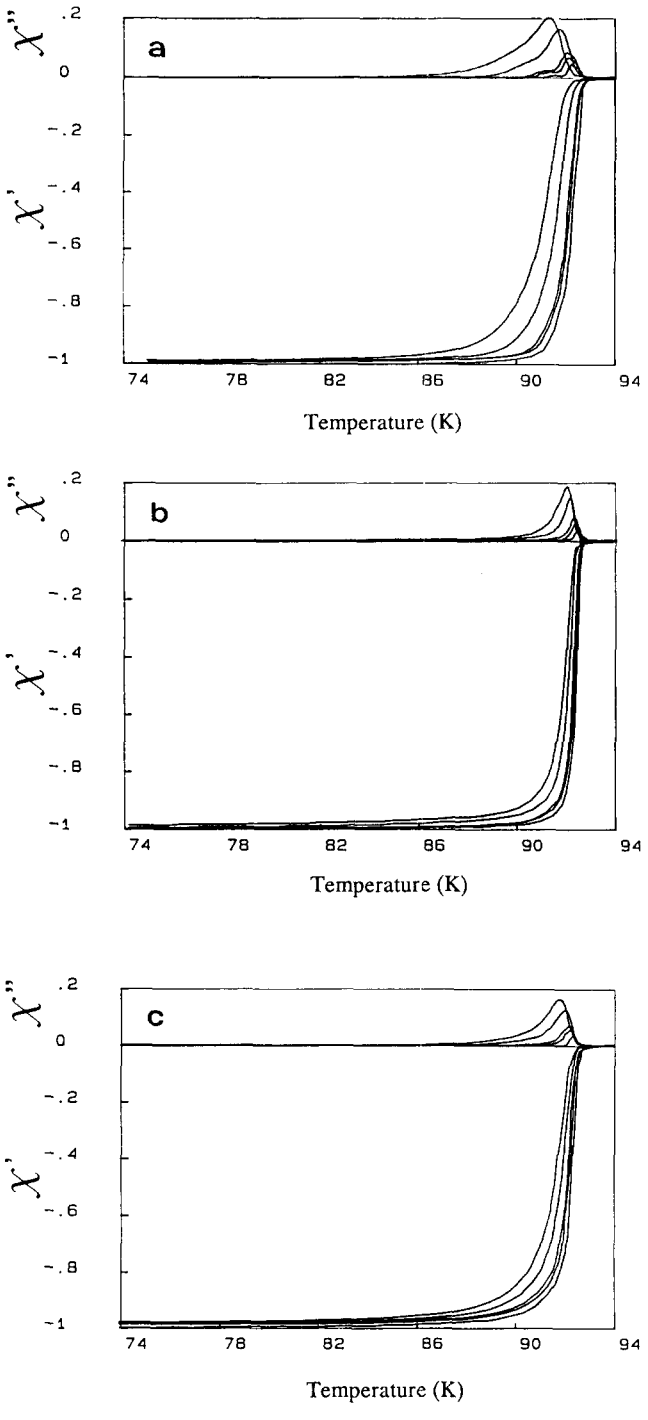

Figure 14 (a) A.c. susceptibility of a type A ceramic for five a.c. induction amplitudes (0.01, 0.05, 0.1, 0.5 and 1 mT). (b) A.c. susceptibility curves of a type B ceramic. (c) A.c. susceptibility curves of a type C ceramic

transition tail. This enlargement is attributed to an oxygen concentration gradient. Results not shown here reveal that annealing under oxygen at 420°C enhances the oxygen concentration homogeneity and leads to a reduction in the transition width, as in type B samples. This behaviour is identical to that observed in as-grown and annealed single crystals: the annealing affects the oxygen distribution more than the maximum oxygen content[18]. The oxygen inhomogeneity can be considered to be the result of the simultaneous existence of

highly oxygenated domains, in accordance with the high onset value of T_c, and of less oxygenated domains, in accordance with the low value of Cu^{3+}. Furthermore in type C materials the large distance observed between production fissures ($d \approx 30$ μm) prevents homogeneous oxidation of the inside of the material.

To evaluate the critical current density of type B samples at liquid nitrogen temperature, the a.c. magnetic induction was increased up to 82 mT. Under such induction, the calculated J_c reaches 12600 A cm^{-2}. *Figure 15* shows the change in J_c with temperature, measured for several amplitudes ($0.01 \leq B \leq 82$ mT). Indirect values of the critical current density have been obtained from magnetization measurements, using a technique developed by Polack *et al.*[19]. At 77 K and applying $B_{a.c.} = 100$ mT, a value of 12960 A cm^{-2} is obtained, very close to the value deduced from a.c. susceptibility.

Direct transport measurements have been carried out on large samples ($30 \times 7 \times 4$ mm^3). Surprisingly, J_c values were low (between 10 and 30 A cm^{-2}) and non-reproducible. Such a result reveals the limited degree of long range texturing. Moreover, the boundaries between the textured domains are large cracks, as in *Figure 13*, reducing the effective current path. Some direct J_c measurements on a single textured domain are currently in progress to validate the previously proposed description of the microstructure.

Conclusions

The production of $YBa_2Cu_3O_{7-\delta}$ ceramics by a controlled melt process, even without an applied thermal gradient, gives rise to a textured material. The microstructure of the resulting ceramics can be described as being composed of large domains which are highly orientated. Beside many impurity grains, parallel fissures reveal the textured nature of the domains. These fissures are probably a result of the production process. The disappearance of part of the liquid phase during the peritectic reaction leads to the formation of crack-like voids (production fissures) between two solidification fronts of $YBa_2Cu_3O_{7-\delta}$. Depending on the starting composition and therefore on the final amount of Y_2BaCuO_5, the distance between these production fissures can change, giving the appearance of random cracks. Addition of CuO-$BaCuO_2$ increases both the average distance between production fissures and the density of these random cracks, but leads to an inhomogeneously oxidized ceramic. A.c. susceptibility measurements show a sharp superconductive transition for all the textured samples. Differences in magnetic induction dependence could be related to two phenomena. For type A ceramics (stoichiometric composition) slight weak link behaviour is observed, which is attributed to the highest density of production fissures which, in turn, are associated with chemical or structural defects. For type C specimens (+10 vol% CuO-$BaCuO_2$) the induction dependence is attributed to oxygen concentration inhomogeneities. A 5% CuO-$BaCuO_2$ addition appears to give the best microstructure. However, with our experimental procedure, long range texturing is not achieved, which prevents us obtaining high values of transport J_c through long samples.

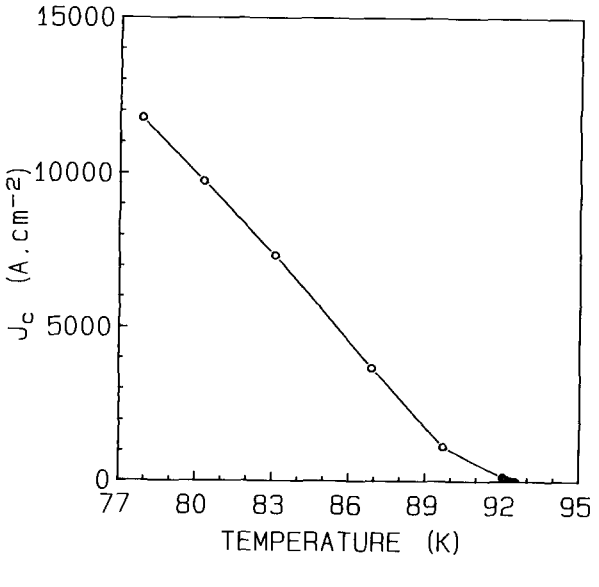

Figure 15 Critical current density of a type B ceramic deduced from a.c. susceptibility measurements using the Bean model

References

1 **Jin, S., Tiefel, T.H., Sherwood, R.C., Davis, M.E. *et al.*** *Appl Phys Lett* (1988) **28** 2074
2 **McGinn, P.J., Black, M.A. and Valenzuela, A.** *Physica C* (1988) **156** 57
3 **Murakami, M., Morita, M., Doi, K. and Miyamoto, K.** *Jpn J Appl Phys* (1989) **28** 1189
4 **Salama, K., Selvamanickam, V., Gao, L. and Sun, K.** *Appl Phys Lett* (1989) **54** 2352
5 **McGinn, P.J., Chen, W. and Black, M.A.** *Physica C* (1989) **161** 198
6 **Murakami, M., Gotoh, S., Koshizuka, N., Tanaka, S. *et al.*** *Cryogenics* (1990) **30** 390
7 **Meng, R.L., Kinalidis, C., Sun, Y.Y., Gao, L. *et al.*** *Nature* (1990) **345** 326
8 **McGinn, P.J., Chen, W., Zhu, N., Balachandran, U. *et al.*** *Physica C* (1990) **165** 480
9 **Murakami, M.** *Mod Phys Lett B* (1990) **4**(3) 163
10 **Pellerin, N.** Crystallization and texturation of YBaCuO *PhD Thesis* Orleans, France (1992)
11 **de Rango, P., Lees, M.R., Lejay, P., Sulpice, A. *et al.*** *Nature* (1991) **349** 770
12 **Lees, M.R., Bourgault, D., Braithwaite, D., de Rango, P. *et al.*** *Physica C* (1992) **194** 171
13 **McGinn, P.J., Zhu, N., Chen, W., Sengupta, S. *et al.*** *Physica C* (1991) **176** 203
14 **Jin, S., Kammlott, G.W., Tiefel, T.H., Kodas, T.T. *et al.*** *Physica C* (1991) **181** 57
15 **Magro, C., Sanz, M., Heintz, J.M. and Bonnet, J.P.** *Compte Rendu Acad Sci* submitted for publication
16 **Chateignier, D.** Pole figure measurements in textured ceramics, personal communication, Paris, France (Oct 1991)
17 **Heintz, J.M., Sanz, M., Wattiaux, A. and Bonnet, J.P.** paper presented at CNRS Colloquium on Microstructure of High T_c Superconductors, Giens, France (June 1989)
18 **Nganga, L., Huong, P.V., Chaminade, J.P., Dordor, P. *et al.*** *J Less Common Metals* (1990) **164/165** 208
19 **Polack, M., Windte, V., Schauer, W., Reiner, J. *et al.*** *Physica C* (1991) **174** 14